Available online at www.sciencedirect.com
ScienceDirect
Geochimica et Cosmochimica Acta 75 (2011) 1992–2006
Geochimica et Cosmochimica Acta
www.elsevier.com/locate/gca

Evidence for wildfire in the Meishan section and implications for Permian–Triassic events

Wenjie Shen [a,c], Yongge Sun [b,c,*], Yangting Lin [a], Dehan Liu [c], Pingxia Chai [c]

[a] Key Laboratory of the Earth's Deep Interior, Institute of Geology and Geophysics, Chinese Academy of Sciences, Beijing 100029, People's Republic of China
[b] Department of Earth Science, Zhejiang University, Hangzhou 310027, People's Republic of China
[c] State Key Laboratory of Organic Geochemistry, Guangzhou Institute of Geochemistry, Chinese Academy of Sciences, Guangzhou 510640, People's Republic of China

Received 30 April 2010; accepted in revised form 12 January 2011; available online 2 February 2011

Abstract

Polynuclear aromatic hydrocarbons (PAHs) and black carbon (BC) in sediments are powerful tools in the identification of the combustion process throughout geologic history. In this study, combustion-derived PAHs and BC were carefully investigated in sediments from the Global Stratotype Section and Point of the Permian–Triassic (P/Tr) boundary in Meishan, China. Quantitative analyses of combustion-derived PAHs and BC demonstrate anomalously high concentrations in the boundary event beds that coincide with the mass extinction horizon. The prevalence of parent polynuclear aromatics (e.g., phenanthrene) in PAHs, together with non-metric multidimensional scaling analysis, confirms that the PAHs are mainly derived from vegetation burning instead of having a coal and/or oil origin. BC detected in sediment occurs in various forms from large irregular charcoal particles to fine aciniform soot, with an equivalent reflectance of up to 3.5%. The results strongly suggest that a wildfire occurred during the P/Tr boundary, which served as one of the possible triggers of mass extinction on land. The wildfire occurrence indicates that the O_2 concentration of the atmosphere during (or before) the P/Tr mass extinction was probably >17%. The temporal coincidence of the mass extinction with intensive volcanic eruption, marine anoxia and wildfire events in the region of the Meishan section provides new insight into the mechanisms of the P/Tr biotic crisis. Our results show that wildfires could have played an important role in the collapse of the ecosystem in the Meishan P/Tr events.

1. INTRODUCTION

It is widely known that the P/Tr boundary event destroyed most marine species, terrestrial vertebrate genera, and most land plants (Erwin et al., 2002). According to the records of marine fossils in the Meishan P/Tr section in China, the mass extinction occurred abruptly (Jin et al., 2000). Though recent studies show that the P/Tr biotic crisis is more protractive or episodic (Xie et al., 2005; Yin et al., 2007), the main mass extinction occurred suddenly in association with the boundary clay, which has been termed "the event beds", including a 3-mm pyrite lamina from bed 24f0, a 4-cm white clay from bed 25, and a 6-cm black mudstone from bed 26 (Jin et al., 2000; Shen and Lin, 2010).

Environmental changes and catastrophic events have been proposed as causes of the great mass extinction (Erwin et al., 2002). To date, however, there is no agreement on the underlying drivers of the P/Tr mass extinction (Cao et al., 2009). One of the most popular theories proposes that

* Corresponding author at: Department of Earth Science, Zhejiang University, No. 38, Zheda Rd, Xihu District, Hangzhou 310027, People's Republic of China. Tel.: +86 0571 86732362.
E-mail address: ygsun@zju.edu.cn (Y. Sun).

0016-7037/$ - see front matter © 2011 Elsevier Ltd. All rights reserved.
doi:10.1016/j.gca.2011.01.027

intense volcanic activity in Siberia led to a global environmental change due to voluminous gases and volcanic ash production (Bowring et al., 1998; Wignall, 2001; Kamo et al., 2003; Mundil et al., 2004; Svensen et al., 2009; Saunders and Reichow, 2009). Furthermore, several studies have suggested that volcanic activity could result in CH_4 release from gas hydrate reservoirs, which could have contribute to marine anoxia and global warming (Krull et al., 2000; Pancost et al., 2007; Retallack and Jahren, 2008). The boundary clay in the Meishan section was confirmed to be of volcanic origin and high-precision U–Pb zircon geochronology showed that the mass extinction was synchronous with the Siberian flood volcanism (Bowring et al., 1998; Wignall, 2001; Kamo et al., 2003; Mundil et al., 2004; Svensen et al., 2009). The platinum-group element patterns in the Meishan P/Tr boundary clay are similar to those of the Siberian flood basalts (Xu et al., 2007). However, the occurrence of high temperature quartz and incompatible element data also indicate a contribution from local acidic to intermediate volcanic eruptions in South China (He et al., 1987; Zhou and Kyte, 1988; Yin et al., 1989) to the boundary clay. Therefore, the genesis of the boundary clay is seemingly more complicated than expected and probably related to multi-type volcanic activity.

Because it is a powerful tool for the delineation of biogeochemical processes in geologic history, in recent years sedimentary organic matter had been used to probe the cause of the P/Tr event. Aryl isoprenoids, isorenieratane and chlorobiaceae derived from green photosynthetic sulfur bacteria (*Chlorobiaceae*), which are prolific at the oxic–anoxic boundary of stratified, sulfide-rich water bodies (Summons and Powell, 1986), have been widely detected in sedimentary organic matter from the P/Tr boundary around the world and indicate an euxinic water column during the P/Tr transition (Grice et al., 2005, 2007). This is consistent with pyrite framboid records (Shen et al., 2007) and earth system modeling results (Meyer et al., 2008). Using one microbial-origin molecule fossil detected in the Meishan P/Tr section (2-methyl hopane (2MHP)), Xie et al. (2005) found two episodes of faunal mass extinction. These episodes likely reflect microbial responses to the catastrophic events that caused the extinction and initiated ecosystem changes. The hopane distributions (Lu and Tong, 2002; Wang, 2007; Xie et al., 2007b; Cao et al., 2009) and aromatic biomarkers (Huang et al., 2006; Wang and Visscher, 2007; Nabbefeld et al., 2010) have also been used to discuss the environmental change and ecosystem collapse at the end of the Permian.

Charcoal deposits, another form of organic matter found in sediments, were recognized throughout the Permian from a variety of ecosystems spreading across a great range of latitudes, which suggests frequent fire occurrences and reflects a relatively high atmospheric oxygen concentration (Wildman et al., 2004; Scott and Glasspool, 2006; Diessel, 2010; Glasspool and Scott, 2010). Previous studies have shown that the atmospheric oxygen reached the highest levels in the Late Paleozoic (Wildman et al., 2004; Scott and Glasspool, 2006), followed by a decline with the smallest O_2 concentration in the Early Triassic (Huey and Ward, 2005; Berner, 2005, 2009; Diessel, 2010; Glasspool and Scott, 2010). At the same time, CO_2 levels rose constantly (Berner, 2005, 2009), resulting in a warmer climate (Huey and Ward, 2005; Kiehl and Shields, 2005; Glikson, 2008; Saunders and Reichow, 2009). Therefore, severe hypoxia seemed inevitable, and this idea has been used to explain the P/Tr land biota crisis (Huey and Ward, 2005; Retallack et al., 2006; Glasspool and Scott, 2010).

Wildfire, a natural phenomenon involving the combustion of carbon materials, is actually a chemical reaction between oxygen and carbon (Scott, 2000). Black carbon (BC), a general term for wildfire residues, is a continuum of combustion products ranging from char, charcoal, and soot to graphitic BC (Hedges et al., 2000; Masiello, 2004). PAHs are also produced during incomplete combustion by gas condensation and are absorbed in BC particles (Simoneit, 2002; Masiello, 2004). The PAH assemblages can also condense into solid spherules with a minimum diameter of 1 nm, which suggests that the presence of PAHs is intrinsic to the structure of soot particles (Kennedy, 1997; Masiello, 2004). BC and PAHs can be used as indicators of ancient wildfires because their relatively inert characteristics are good for long-term preservation (Jiang et al., 1998; Masiello and Druffel, 1998; Scott, 2000; Finkelstein et al., 2005; Belcher et al., 2009; Marynowski and Simoneit, 2009; Scott and Damblon, 2010).

Several studies indicate the possibility of wildfires having occurred during the depositional interval of the P/Tr boundary (Chijiwa et al., 1999; Wang and Yin, 2001; Wang and Chen, 2001; Thomas et al., 2004; Grice et al., 2007; Uhl et al., 2007; Cao et al., 2008; Shen et al., 2008; Nabbefeld et al., 2010; Scott, 2010; Uhl and Montenari, 2010). In geologic history, abundant charcoal particles are widely detected and preserved in sediments throughout the Permian, suggesting that wildfires were frequent at that time. Further studies have indicated that, through the Permian, the intensive, global volcanic activities were a significant cause of wildfires (Scott, 2000; Scott and Glasspool, 2006; Diessel, 2010). Wildfires will undoubtedly result in environmental change (Page et al., 2002; Bowman et al., 2009; Marlon et al., 2009) and ecosystem disasters (Abram et al., 2003; Huey and Ward, 2005). Because of oxygen limits on combustion, in contrast, combustion products preserved in sediments can serve as direct indicators of past atmospheric O_2 concentrations (Jones and Lim, 2000; Wildman et al., 2004; Belcher and McElwain, 2008).

Our preliminary investigation demonstrated a significantly high BC content in event bed 26 from Meishan, China. This BC content is a possible indicator of wildfires during the P/Tr boundary event bed interval (Shen et al., 2008). In this paper, we focus on the combustion-derived PAHs for further evidence of the wildfire. High-resolution sampling in the Meishan P/Tr section in the Zhejiang province of China was performed, and various forms of BC particles (including charcoal morphology) that were detected in sediments were also carefully examined using a scanning electron microscope. This study aims to probe wildfire dynamics at the P/Tr boundary and the possible relationship with the mass extinction.

2. MATERIALS AND METHODS

2.1. Geologic setting and samples

The Meishan section, one of the most extensively examined sections around the world with respect to the P/Tr biotic crisis, is located in South China and was defined as the Global Stratotype Section and Point (GSSP) of the P/Tr boundary in 2001 (Jin et al., 2000; Yin et al., 2001). The Meishan section developed in an intra-platform depression between the Niutoushan SW–NE uplift and a platform in the northeastern Tethys. The section exhibits transitional facies from the platform to the slope during the P/Tr interval (Yin et al., 2001), showing dysoxic depositional conditions as revealed by lithology, paleontology and mineral records (Wignall and Twitchett, 2002; Shen et al., 2007; Bond and Wignall, 2010). The deposition rates, calculated from zircon U–Pb ages of the ash beds (Bowring et al., 1998), are 0.03 cm per 1000 years for the transitional beds (beds 25–28) (Jin et al., 2000), suggesting a slow sedimentation process during the P/Tr boundary interval. This has also been shown by extensively burrowed hardgrounds within bed 27 (Cao and Zheng, 2009).

The lithology of the profile across the P/Tr boundary is characterized by calcareous mudstone (beds 24, 27) with a thin yellow–brown pyrite lamina at the top of bed 24 (bed 24f0), pale-colored, ash clay stone (beds 25, 28), a laminated organic-rich calcareous clay stone (bed 26), and grey organic-rich shale, which is pale marl or muddy limestone (beds 29, 30). Bed 27 marks the P/Tr boundary, which was indicated by the first appearance of *Hindeodus parvus* (Yin et al., 2001, 2005). The faunal mass extinction occurs at beds 25–26, indicated by the well-established faunal stratigraphic distributions (Jin et al., 2000). Together with bed 24f0, beds 25 and 26 are usually defined as key event beds, and they were directly followed by the P/Tr boundary mudstone deposits (bed 27). Twenty samples were collected for geochemical analyses from bed 24d to bed 30 (where beds 24d–24e belong to the Changhsing Formation and beds 24f0–30 belong to the Yinkeng Formation) at the fresh surface outcrops in quarry C of the Meishan section. A simple continuous inequidistant sampling method was applied in beds 25 and 26, where 10 specimens (MSC25a to MSC25g and MSC26a to MSC26e, Tables 1 and 2) were collected in total. These samples were carefully handled to avoid contamination and were ground into powders for organic matter extraction and BC separation. Large blocks of samples from bed 25 and bed 26 (1.2 and 1.3 kg, respectively) were also used for charcoal investigations.

2.2. Methods

2.2.1. Rock–Eval pyrolysis

Rock–Eval pyrolysis was performed first to obtain the T_{max} value, which is a standardized parameter used to evaluate maturity of sedimentary organic matter. To summarize briefly, 50–100 mg whole-rock powder samples were loaded onto a Rock–Eval 6-standard instrument, where a pyrolysis process with a standard oven temperature program was conducted. Sedimentary organic matter was pyrolyzed and detected by a flame ionization detector (FID). The results included S1, S2, TOC, and T_{max}, which represent the free hydrocarbons distributed in the sediments, kerogen pyrolysis products, total organic carbon, and maximum temperature of peak yields during kerogen pyrolysis.

Table 1
Results of Rock–Eval analysis of sediments from the Meishan section.

Samples	System	R_c	TOC	T_{max}	S1	S2	PI	HI
MSC30	T1	0.81	0.49	485	0.00	0.00	0.68	0
MSC29	T1	0.75	0.86	427	0.00	0.01	0.11	1
MSC28	T1	1.12	0.10	376	0.03	0.00	1.00	0
MSC27cd	T1	1.01	0.14	387	0.01	0.00	0.72	3
MSC27ab	P2	1.01	0.16	386	0.02	0.01	0.67	3
MSC26e	P2	0.79	0.56	428	0.02	0.3	0.07	54
MSC26d	P2	0.72	0.94	433	0.04	0.73	0.05	78
MSC26c	P2	0.75	1.16	434	0.05	0.78	0.06	67
MSC26b	P2	0.74	0.81	431	0.03	0.57	0.06	70
MSC26a	P2	0.77	0.82	431	0.04	0.58	0.07	71
MSC25g	P2	0.79	0.82	430	0.05	0.57	0.08	70
MSC25f	P2	0.80	0.54	427	0.03	0.29	0.10	55
MSC25de	P2	0.85	0.34	427	0.03	0.12	0.20	35
MSC25bc	P2	0.94	0.18	430	0.01	0.02	0.33	11
MSC25a	P2	1.09	0.09	425	0.03	0.00	0.98	0
MSC24f0	P2	0.90	0.19	429	0.00	0.00	0.24	0
MSC24ec	P2	0.71	0.97	439	0.02	0.61	0.03	63
MSC24eb	P2	0.81	0.59	445	0.00	0.05	0.06	8
MSC24ea	P2	0.84	0.44	441	0.01	0.10	0.05	23
MSC24d	P2	1.06	0.56	485	0.00	0.04	0.03	7

Notes: R_c values were calculated by the methyl phenanthrene index (%); TOC: total organic carbon (wt.%); T_{max}: temperature at which the S2 peak reaches its maximum (°C); S1: free hydrocarbons (mg HC/g rock); S2: oil potential (mg HC/g rock); PI: production index; HI: hydrogen index.

Table 2
Quantitative results of selected combustion-derived PAHs from sediments in the Meishan section (ng/g of rock). Note a rapid increase of BC and PAH concentrations in event beds (from the lowest in the bottom of bed 25 to the highest in the middle of bed 26).

Samples	System	BC (%)	Phe	Pyr	Chy	BF	BeP	BaP	InP	BPery	Cor	Total*
MSC30	T1	0.0347	64	25	13	10	15	1	1	6	2	137
MSC29	T1	0.0409	90	33	19	13	20	1	1	8	3	189
MSC28	T1	0.0143	137	106	8	5	6	0	0	0	0	262
MSC27cd	T1	0.0330	86	71	9	8	10	1	1	6	4	196
MSC27ab	P2	0.0218	96	59	6	3	5	1	0	5	10	186
MSC26e	P2	0.2530	735	249	95	78	132	19	12	79	23	1422
MSC26d	P2	0.4310	870	330	156	118	208	31	18	134	24	1888
MSC26c	P2	0.5104	1078	568	189	168	283	46	21	137	19	2509
MSC26b	P2	0.3365	732	499	152	122	206	34	14	82	11	1853
MSC26a	P2	0.3381	972	636	153	125	218	34	14	82	10	2244
MSC25g	P2	0.3063	241	236	25	68	112	16	7	38	4	746
MSC25f	P2	0.1788	167	149	17	41	69	10	4	22	2	481
MSC25de	P2	0.0999	154	116	12	20	34	5	1	9	1	352
MSC25bc	P2	0.0375	123	91	6	8	12	2	1	3	0	245
MSC25a	P2	0.0108	22	19	2	2	4	1	0	0	0	48
MSC24f0	P2	0.0621	69	45	9	9	11	3	1	4	1	152
MSC24ec	P2	0.1961	155	454	31	67	73	24	8	24	4	840
MSC24eb	P2	0.0266	54	56	7	9	8	2	1	5	2	144
MSC24ea	P2	0.0521	92	72	9	14	11	3	1	5	1	209
MSC24d	P2	0.1546	54	6	26	8	4	0	0	1	1	100

Notes: BC data from Shen et al. (2008). Name abbreviations: Phe, phenanthrene; Pyr, pyrene; Chy, chrysene; BF, benzo[bjk]fluoranthene; BeP, benzo[e]pyrene; BaP, benzo[a]pyrene; InP, Indeno[cd]pyrene; BPery, benzo[ghi]perylene; Cor, coronene, hereinafter the same; *, total selected PAHs.

2.2.2. PAH analysis

Samples of 6–20 g were extracted using a Soxhlet apparatus for 72 h with dichloromethane/methanol (97:3, v:v). Dilute-HCl activated copper was used to remove elemental sulfur from the extracts. The extracts were then concentrated and dried with a rotary evaporator under reduced pressure. Asphaltenes were removed by precipitation with *n*-hexane and then filtered. The de-asphaltened fractions (maltene) were then separated into aliphatic, aromatic, and polar (NSO) fractions by micro silica–alumina column (60 × 8 mm) chromatography (Xu and Sun, 2006), using hexane, benzene, and ethanol as solvents, respectively.

Aromatic hydrocarbon fractions were analyzed by GC–MS using a Micromass Platform II mass spectrometer coupled to a Hewlett–Packard 6890 gas chromatograph. Chromatographic separation was achieved with a 60 m × 0.32 mm i.d. fused silica capillary column coated with a 0.25 μm film of HP-5MS. The oven temperature program started at 70 °C (3 min), and then rose to 290 °C at 3 °C/min, followed by a 30 min hold. Helium was used as the carrier gas with a flow rate of 1.0 ml/min. The transfer line temperature was 250 °C, and the ion source temperature was 200 °C. The ion source was operated in the electron impact (EI) mode at 70 eV. Full scan (50–550 amu) was used to identify the compounds of interest. The identification of compounds was based on the retention time with reference compounds and comparison of data published in literatures. The quantitative analyses of PAHs were conducted by comparing the peak areas of corresponding mass chromatograms with those of known amounts of internal reference compounds (deuterated PAHs, including naphthalene-d8, acenaphethene-d10, phenanthrene-d10, chrysene-d12 and perylene-d12) that were added to the samples before extraction.

2.2.3. BC observations and reflectance measurements

Because of the relatively incoherent character of the clay (bed 25) and mudstone (bed 26), these samples were decomposed by a freeze/thaw method. Large blocks of beds 25 and 26 were first soaked in deionized water and decomposed by a process of freeze/thaw cycles (total cycles >20), followed by a wet-sieving separation with different meshes (40, 100, 200 and 500 mesh, in turn). In many cases, there was an excess of pyrite in the fraction of 200–500 mesh, which likely affected the BC observations. Therefore, the fraction of 200–500 mesh was purified using dense liquors to eliminate the pyrite. The pyrite-free portion of the 200–500 mesh fraction, together with the fraction of >200 mesh, was deposited on glass slides with a thin layer of glue for BC observation. A LEO 1450VP scanning electron microscope equipped with an energy dispersive X-ray detector was used in this study.

To determine the reflectance, BC particles were isolated and purified from the powdered samples. The pre-treatment methods used in this study include the dissolution of carbonates by 3 M HCl and the dissolution of silicates by 10 M HF, followed by 0.1 M $K_2Cr_2O_7$/2 M H_2SO_4 to eliminate kerogen. The residue was attached to the glass using 502 glue and then polished. The BC charcoal reflectance measurement was made on the polished thin sections with a Leica MPV3 microphotometer. Polarized reflected light was used to measure the mean random percentage reflectance in oil (reflective index of 1.515 at 26 °C).

3. RESULTS

3.1. The PAHs

Rock–Eval pyrolysis revealed that the T_{max} values of the samples ranged from 376 to 445 °C, with two exceptions with values of 485 °C (beds 24d and 30, Table 1), indicating a marginally mature to mature stage. These measurements are consistent with the equivalent vitrinite reflectances, R_c (0.71–1.12%), which were calculated from the methyl phenanthrene index. The sediment's thermal history suggested that it is usable for molecular geochemistry investigation, following the procedures previously demonstrated by Huang et al. (2006), Wang (2007) and Xie et al. (2005). In this study, phenanthrene (Phe), pyrene (Pyr), chrysene (Chy), benzo[bjk]fluoranthene (BF), benzo[e]pyrene (BeP), benzo[a]pyrene (BaP), Indeno[cd]pyrene (InP), benzo[ghi]-perylene (BPery) and coronene (Cor) were selected as indicators to examine biomass burning.

Although the distribution of PAHs in sedimentary organic matter from the P/Tr boundary in Meishan is usually dominated by 3 and 4 ringed polynuclear aromatic hydrocarbons, there is a notable accumulation of 5 and 6 ringed PAHs in the studied sample, especially in sedimentary organic matter from event bed 26 (Fig. 1 and Table 2). The quantitative analyses of PAHs show that there is a significantly high concentration peak in sediments in bed 26 (Table 2, Figs. 1 and 2). The concentration of the total selected PAHs in bed 26 (MSC26c) is 12 times greater than what is seen in beds 27–30 and 7 times the concentrations of beds 24d–25. In Fig. 2, all of the selected PAHs demonstrate the same pattern, showing pronounced peaks in bed 26. This pattern is exactly like what was previously observed from the BC concentration profile (Shen et al., 2008). In the PAH concentration profile, there is another small peak in the upper part of bed 24e, just beneath the boundary event layer (beds 24f0–26). Other layers have very low concentrations of PAHs.

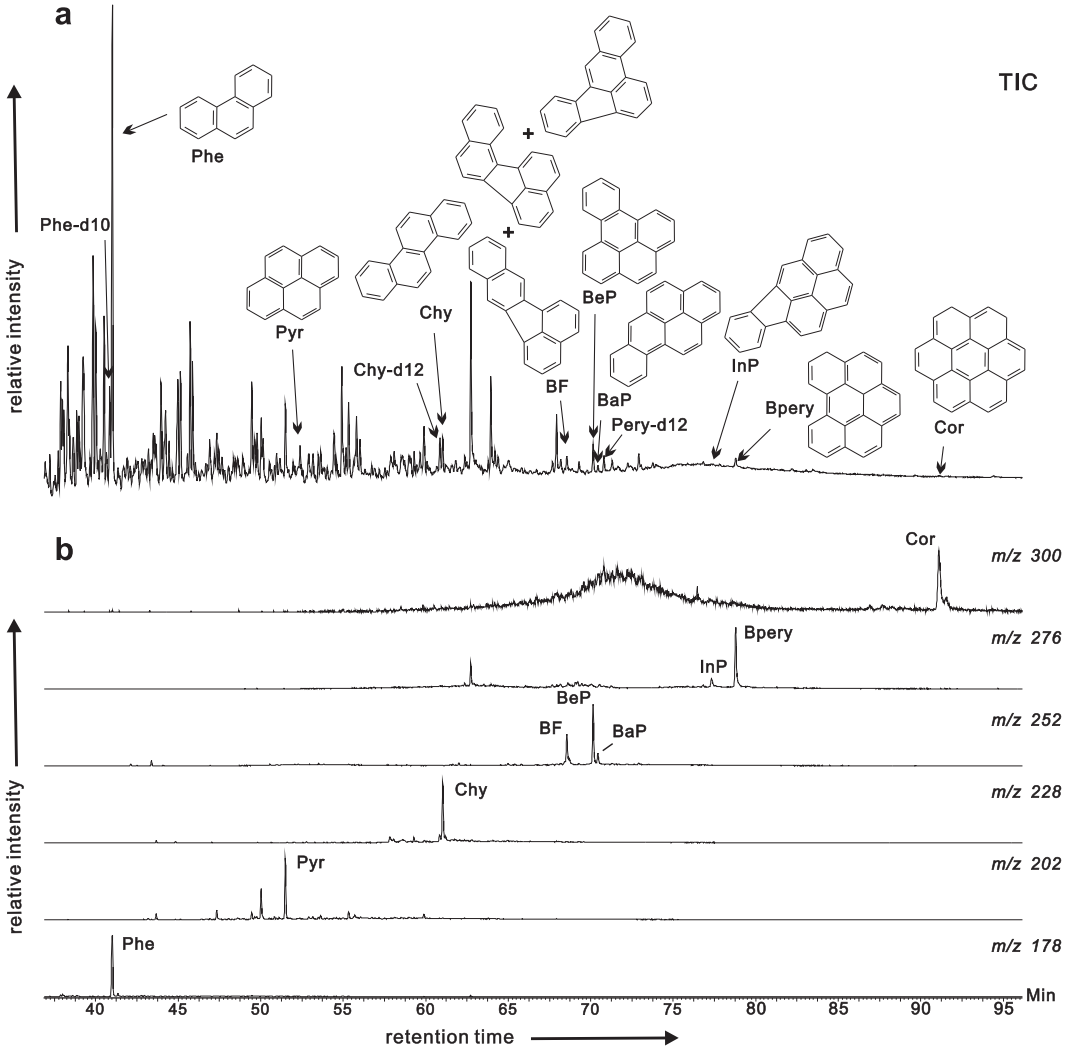

Fig. 1. Partial TIC (total ion chromatogram) trace (a) and mass chromatogram of selected combustion-derived PAHs (b) from GC/MS analysis of an aromatic fraction of sample MSC26b. Name abbreviations: Phe-d10, phenanthrene; Chy-d12, chrysene-d12; Pery-d12, perlene-d12.

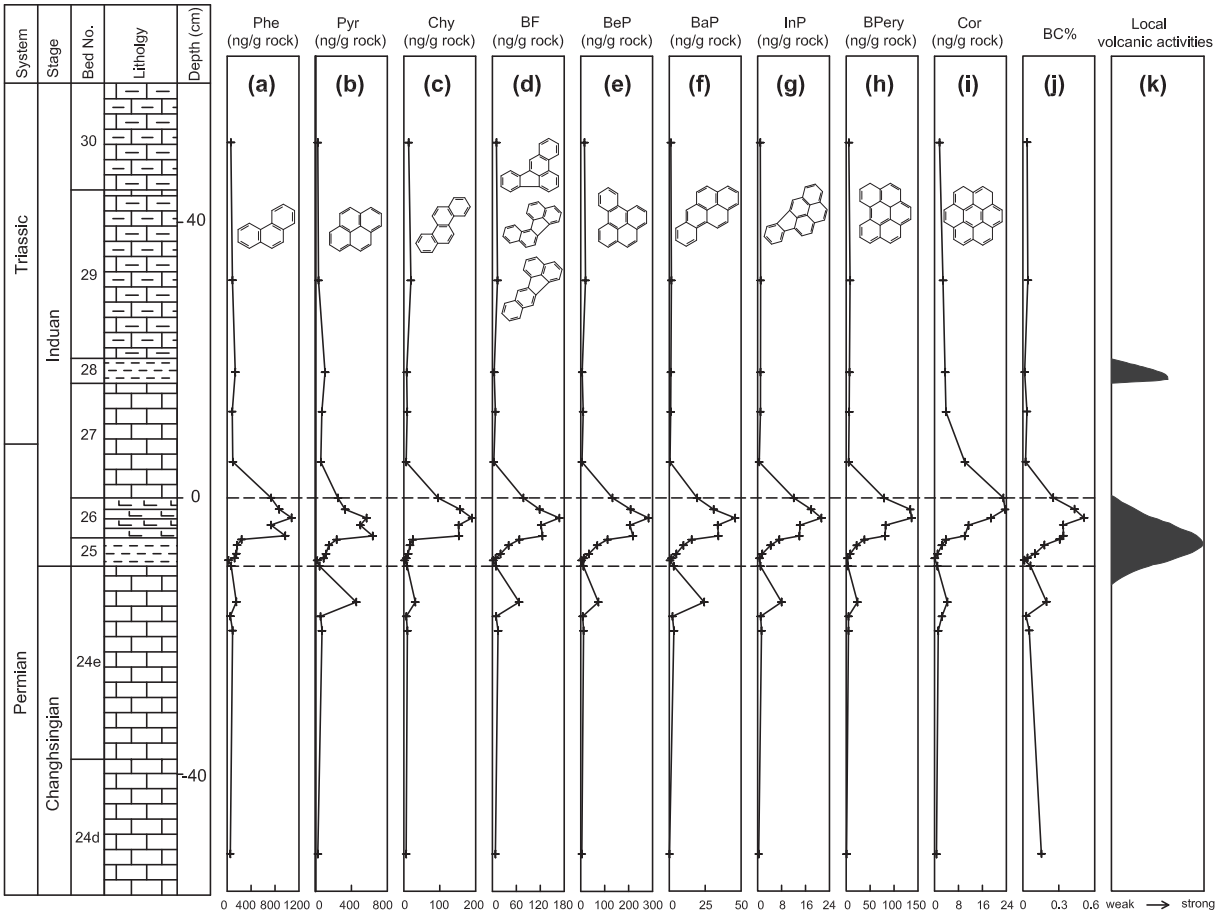

Fig. 2. Stratigraphic variation across the P/T boundary at Meishan section for selected combustion-derived PAH concentrations (ng/g of rock). (a) Phe; (b) Pyr; (c) Chy; (d) BF; (e) BeP; (f) BaP; (g) InP; (h) BPery; (i) Cor; (j) BC content from Shen et al. (2008); (k) the relative intense volcanic activities from (He et al., 1987). The two dashed lines bracket the P/Tr mass extinction interval coinciding with local volcanic activity and main Siberian trap volcanism (Kamo et al., 2003), and also cover the peaks of combustion-derived PAHs and BC in Meishan section.

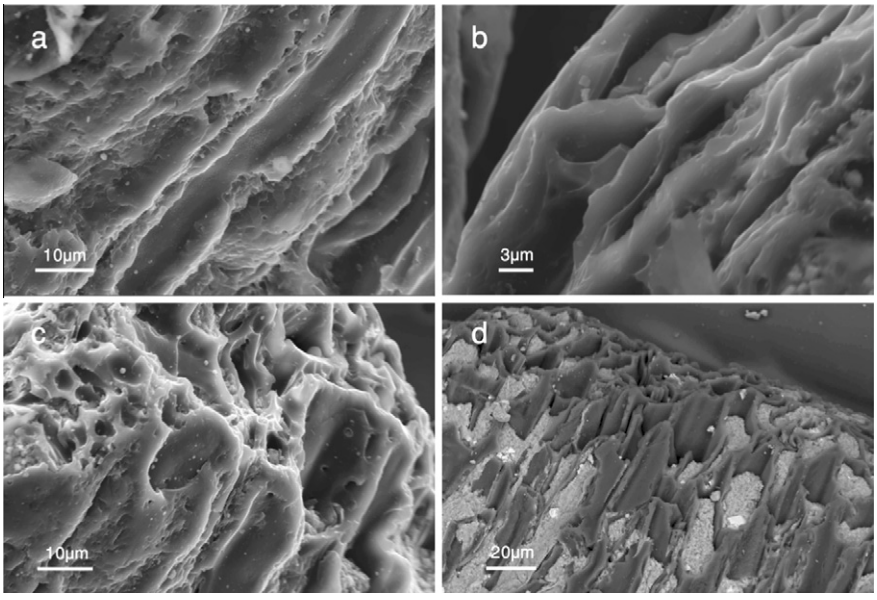

Fig. 3. Scanning electron micrographs of BC charcoal particles with plant's anatomy in bed 25 in Meishan P/Tr section. All these photos exhibit homogenized cell walls and tracheids. (a–c) Secondary electron (SE) images. (d) Backscattered electron (BSE) image.

3.2. BC morphology and reflectance

Four types of BC morphologies can be identified in the Meishan section samples. (1) Charcoal particles with plant cellular structure are relatively large in size (usually >100 μm, with the largest at 250 × 750 μm; Fig. 3). The homogenized cell walls and tracheids in charcoal particles were well preserved and can still be clearly recognized; (2) Columnar or irregular charcoal particles without plant cellular structure are relatively small in size and most of them are less than 100 μm in size (Fig. 4a, c and e). One of the most impressive characteristics is that some of the charcoal particles are impregnated with aciniform soot (Fig. 4e); (3) Smooth spherules with diameters from several microns to ~50 μm (Fig. 4b, d and e); and (4) aciniform soot in form of loose aggregates with very fine particles (Fig. 4d and e).

In summary, BC particles in the Meishan P/Tr section are relatively small in size (less than 1 mm) and are found in various forms from charcoal to soot. The spherules larger than 5 μm in diameter (Fig. 4b, d and f) are actually cenospheres, which are similar to those found at the K/Pg boundary (Harvey et al., 2008). It is interesting to note that aciniform soot is embedded within the body of the charcoal particles (Fig. 4e) and that pyrite framboids are also directly deposited on the surface (or in the holes and surface cracks) of the charcoal fragments (Figs. 3d, 4c and e) and cenospheres (Fig. 4b).

The equivalent reflectance values from 125 analytical points in charcoal particles from bed 26 (MSC26c) have a wide range from 0.5% to 3.5%, with a mean value of $1.1 \pm 0.8\%$ (1σ). As seen in Fig. 5, the equivalent reflectances demonstrate an abnormal distribution with several

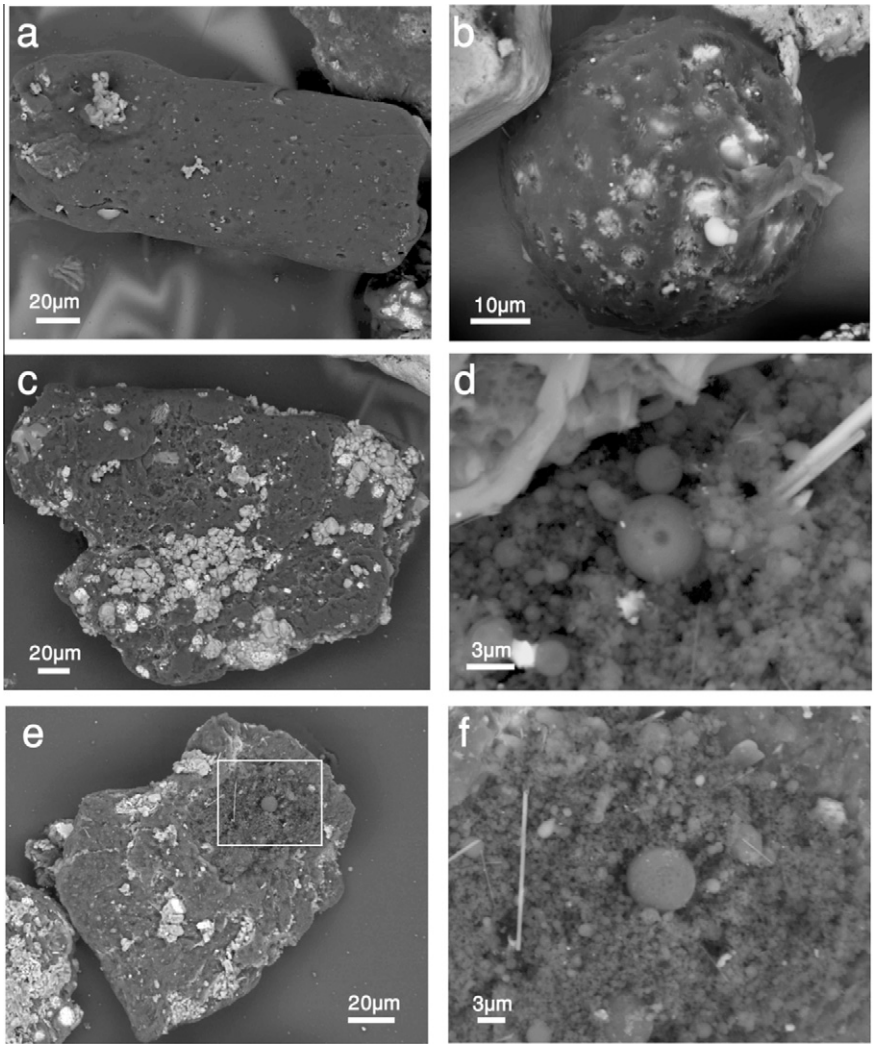

Fig. 4. BSE images of Black carbon fragments from event beds in the P/T boundary section in Meishan. (a) Charcoal particles without preservation of plant anatomy from bed 25. (b) BC spherule with relatively large diameter (~50 μm) from bed 25. Note the smooth surface shows holes that are partly filled with pyrite framboids. (c) An irregular charcoal particle with bright pyrite framboids and partly oxidized gray pyrite from bed 25. (d) Aciniform soot with a 5 μm spherule from bed 26. Note that the 5 μm spherule showing smooth surface. (e) Charcoal particle from bed 26. Note the growth of aciniform soot (square) on the squarish charcoal particle. (f) Magnification of the square area indicated in (e).

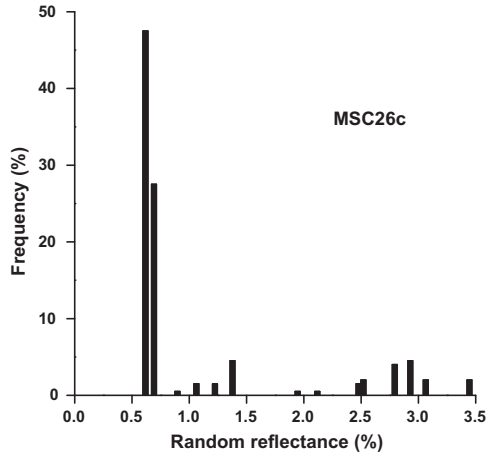

Fig. 5. Histogram of reflectances measured at random sites on the polished BC charcoal particles from bed 26 (under oil).

peaks. This characteristic is similar to what has been observed in the K/Pg charcoal particles (Jones and Lim, 2000) and is consistent with typical reflectance values of charcoal formed by modern, scrubby woodland fires and conifer forest fires (Jones et al., 1991; Scott and Jones, 1994).

4. DISCUSSION

4.1. Wildfire records in the Meishan section

4.1.1. The PAHs

The interpretation of the PAH data must seriously consider the preservation conditions, including the thermal history, biodegradation and weathering (Venkatesan and Dahl, 1989; Jiang et al., 1998). Rock–Eval pyrolysis shows a mild thermal history at the Meishan section, which favors the preservation of organic matter. Previous studies suggested that an anoxic depositional environment was prevalent across the P/Tr transition in the Meishan section, which is supported by facies (Wignall and Twitchett, 2002), pyrite framboid (Shen et al., 2007), sulfur isotopes and biomarkers (Grice et al., 2005). In this case, biodegradation was constrained in the Meishan section and the biomarkers are well preserved, especially for the highly pericondensed PAHs, which are stable due to their ringed structure (Venkatesan and Dahl, 1989; Jiang et al., 1998; Arinobu et al., 1999; Finkelstein et al., 2005; Scott et al., 2010). In addition, samples collected from fresh outcrops ensure less influence from weathering.

Combustion products are characteristically dominated by parent PAHs, whereas alkylated PAHs dominate in bitumen and petroleum (Venkatesan and Dahl, 1989). The elevated abundance of parent Phe in bed 26 is distinct from that in bed 24ec (Fig. 6) in the Meishan section, which possibly indicates combustion material input to the boundary layer. Highly pericondensed PAHs (e.g., BeP and BPery) are typical pyrosynthetic compounds formed by forest fire and organic combustion, and they stabilize in post-depositional conditions (Jiang et al., 1998; Arinobu et al., 1999), particularly under dysoxic to anoxic conditions (Shen et al., 2007). The distribution and relatively high concentrations of polynuclear PAHs, especially with 5, 6 and 7 ringed PAHs in the Meishan P/Tr sediments are consistent with high temperature wildfires (Jiang et al., 1998; Finkelstein et al., 2005; Scott et al., 2010). These data support the occurrence of moderate to intensive forest wildfires at the P/Tr boundary.

The PAH data from the Meishan section, together with a PAH data base from combustion of bituminous and lignite coal (Oros and Simoneit, 2000), oil and diesel (Li et al., 1999), gymnosperms (Oros and Simoneit, 2001), and K/Pg samples (Belcher et al., 2009), are used for non-metric multidimensional scaling analysis. As seen in Fig. 7, the analysis clearly reveals that all of the Meishan samples, except MSC24ec, are grouped with gymnosperms, suggesting a close relationship. Because of the large distance to other sample groups in Fig. 7, the Meishan data can not be grouped with lignite coal, bituminous coal, diesel or oil. They also are very different from the values of K/Pg samples (the ejecta layer, fireball layer and reworked layer), indicating a difference in origin, which is consistent with the disaccord in the 5 and 6 ringed PAH distributions between the Meishan P/Tr and the K/Pg samples (Belcher et al., 2009). The inner distances between the group members can largely be explained by the variations in lithology. MSC24ec is located in the upper left area of the plot, far away from other samples, which is consistent with its

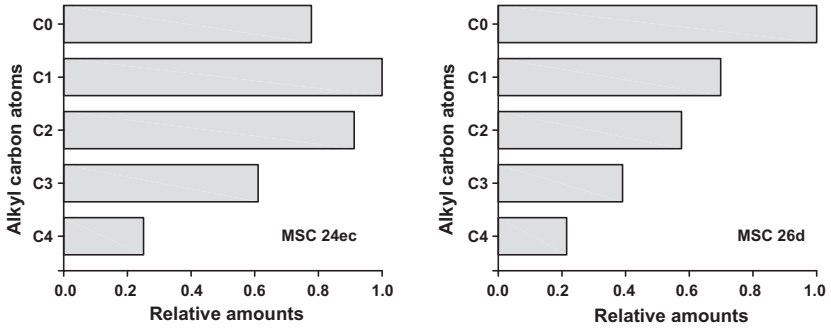

Fig. 6. Alkyl homologue distributions of phenanthrenes (Phe) from bed 26 and bed 24e. The most abundant homologue in each sample is set to 1.0. It probably shows the different origin of PAHs. The predominance of parent Phe in MSC26d likely indicates a combustion origin, where as alkylated Phe in MSC24ec reveals a prime origin of bitumen and petroleum.

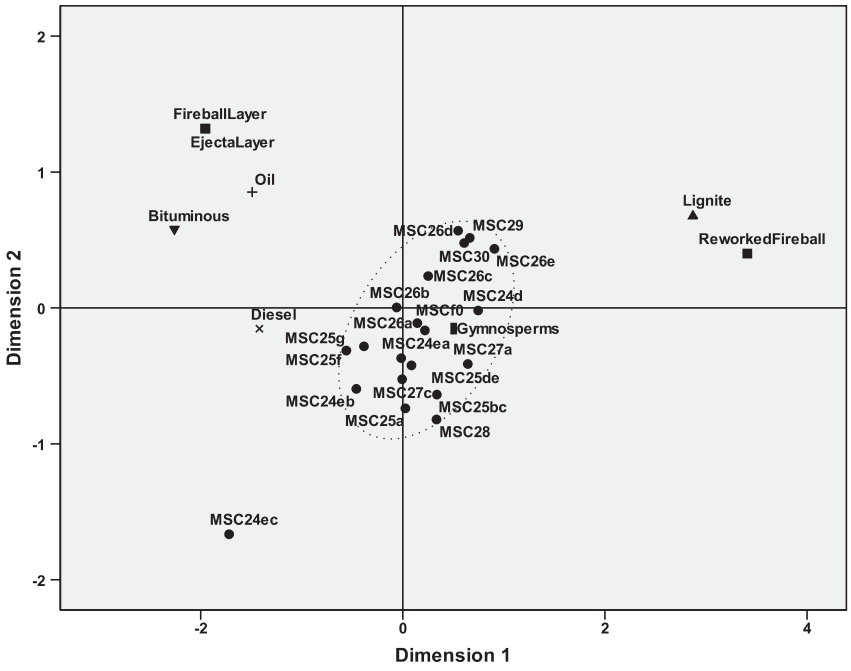

Fig. 7. Non-metric multidimensional scaling analysis of different combustion materials compared with PAHs from Meishan P/Tr section. This figure was plotted by *spss* software with the method of non-metric multidimensional scaling. The raw data were normalized by variable mean and the distance was measured by the Minkowski (3) method. The stress value (0.05) is fair according to Kruskal's experience (Kruskal, 1964). The stress and squared correlation (RSQ) value reaches 0.99 suggesting a high explanation ability. Source data of bituminous coal and lignite coal, oil and diesel, gymnosperms, and K/Pg samples are from Li et al. (1999), Oros and Simoneit (2000, 2001), and Belcher et al. (2009), respectively.

relatively high abundance of alkyl homologue distributions of Phe (Fig. 6).

4.1.2. BC

BC charcoal particles are preserved in the clay and mudstone layers in beds 25 and 26. Charcoal fragments with moderate abrasions usually have diameters of <1 mm (Fig. 4a, c and e). This result suggests that the particles might have experienced transportation over a considerable distance, which is in agreement with the sedimentological setting for the charcoal-bearing beds as marine, with a platform to slope deposition (Yin et al., 2001). The co-occurrence of pyrite framboids and BC fragments observed in the Meishan P/Tr section indicates that the dysoxic depositional environment played an important role in long-term preservation of the BC particles (Figs. 3d, 4b, c and e).

All of the charcoal particles identified with plant cell structures have pycnoxylic wood with tracheid diameters of 10–20 μm (Fig. 3). The rays are triseriate and the pits seem accidental with oval to round morphology (Fig. 3c). These characteristics are not the typical anatomy due to the broken nature of the charcoal fragments, along with the influence of the charring process. Therefore, it is still ambiguous whether the observed character is actually a reliable taxonomic feature or an artifact of charring. Further detailed studies are needed to probe their nature and specific affiliation.

BC particles, including charcoal, cenospheres and soot, should be a direct record of wildfires in the Meishan P/Tr section. In most cases, a given charcoal particle is impregnated with soot (Fig. 4e), and the co-occurrence likely reveals a close relationship in the origin of the charcoal and the soot. For example, BC charcoal and soot were likely produced by a similar wildfire, before being transported and deposited together.

The relationship between charcoal reflectance and combustion temperature has been investigated for a long time (Jones et al., 1991; Scott and Jones, 1994) and new developments have occurred in recent years (Scott and Glasspool, 2005; McParland et al., 2007, 2009; Ascough et al., 2010; Scott, 2010). According to the correlation curve between the temperature and charcoal reflectance constructed by Scott (2010), the formation temperature of BC charcoal in the Meishan P/Tr boundary section was estimated between 310 and 520 °C, which is consistent with modern wildfires (Finkelstein et al., 2005).

4.1.3. Other possible wildfire records in the Meishan section

Xie et al. (2007a) analyzed the concentration variation of charcoal particles using microscopic images and found two episodic changes of BC abundance with peaks in bed 26 and beds 30–34, corresponding to two stages of the P/Tr mass extinction. They argued that volcanism-related wildfires might contribute to the presence of the BC that was transported into the marine sediments along with the higher plant materials.

Fullerenes can be formed in flames during incomplete combustion, although it is difficult to be preserved during burning processes in natural labs (Gerhardt et al., 1987; Howard et al., 1991; Alford et al., 2008). Normally, the

concentration of fullerenes in the remaining soot will be very small (Kratschmer, 2006). Fullerenes have been extracted from wood charcoal and served as evidence for wildfires (Heymann et al., 1994; Shibuya et al., 1999; Chijiwa et al., 1999; Heymann et al., 2003; Li et al., 2005). There are several reports associated with the detection of fullerenes in the Meishan P/Tr sediments (Becker et al., 2001; Li et al., 2005; Shen et al., 2006). However, it is still strongly debated whether the fullerenes are of impact origin or of wildfire origin. The argument for an impact origin of the fullerenes has been criticized due to experimental procedure and unduplicated results (Braun et al., 2001; Farley et al., 2001, 2005). Furthermore, to date there is no other convincing evidence for an impact event at the P/Tr boundary (Farley et al., 2001; Koeberl et al., 2004). Most likely, the fullerenes in the Meishan P/Tr boundary sediments are of combustion origin and, therefore, indicate wildfire events.

4.2. Wildfire records in global P/Tr sections

Chijiwa et al. (1999) detected 10–20 ppt of fullerenes at the P/Tr boundary in central Japan, and they proposed that the fullerenes were likely synthesized in extensive wildfires and deposited in an anoxic marine environment of the superocean Panthalassa. High charcoal and wood fragment content was also found in the upper Permian sediments in the Perth basin of western Australia (Thomas et al., 2004). This finding is in agreement with the abundant unsubstituted PAHs identified from the same sediments (Grice et al., 2007), suggesting a wildfire occurred at the end of the Permian in west Australia. Charcoal particles were also recognized in terrestrial sequences in the SLA section of Xinjiang, in NW China (Cao et al., 2008), the Zhejue and Chahe sections in Guizhou of SW China (Wang and Yin, 2001), the Beode section in Shanxi, North China (Wang and Chen, 2001) and in the Late Permian Um Irna Formation in Jordan (Uhl et al., 2007). More recently, Nabbefeld et al. (2010) measured PAHs in three P/Tr sections from the Meishan, the Kap Stosch area (East Greenland), and the Peace River Basin (Western Canada) that revealed enhanced combustion-derived PAHs concentration. These observations, thus, further support the possibility of a wildfire occurring at the P/Tr boundary.

Although more detailed and dedicated studies are needed to examine the distribution and origin of wildfire evidence at the P/Tr boundary around the world, fullerenes, charcoal particles and PAHs from Paleo-Tethys, Neo-Tethys, Gondwana and Panthalassa are widely documented, and thus wildfires have likely been a common phenomenon during the P/Tr transition (Chijiwa et al., 1999; Wang and Yin, 2001; Wang and Chen, 2001; Thomas et al., 2004; Grice et al., 2007; Uhl et al., 2007; Cao et al., 2008; Shen et al., 2008; Nabbefeld et al., 2010; Scott, 2010; Uhl and Montenari, 2010).

4.3. Wildfire implications for P/Tr events

4.3.1. High-resolution integrated profile across the mass extinction horizon

The main P/Tr mass extinction, mentioned above, occurred in conjunction with many related events recorded in the boundary sediments in the Meishan section (Jin et al., 2000; Shen et al., 2010). A high-resolution integrated profile across the mass extinction horizon in the Meishan section (Fig. 8) reveals that large quantities of volcanic materials, including quartz, orthoclase, zircon and altered glass shards, abruptly appear in the upper part of the pyrite crust (i.e. pyrite lamina) with the disappearance of marine species (Shen et al., 2010). An anoxic depositional environment prevailed in the pyrite crust and above layers of beds 25–26, indicated by the occurrence of pyrite framboids

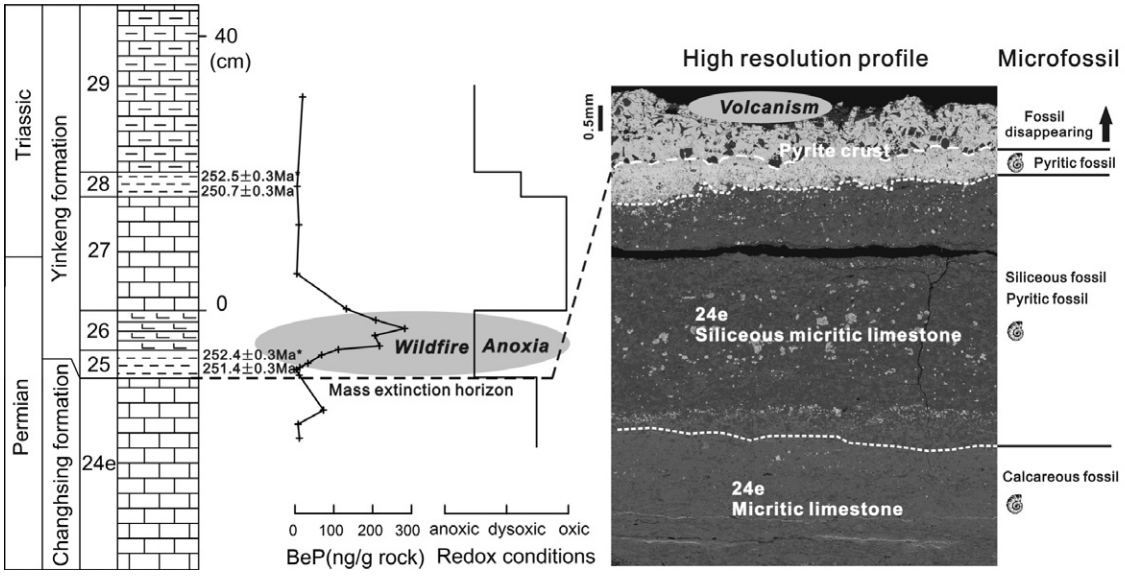

Fig. 8. High resolution profile across the mass extinction horizon in the Meishan P/Tr section. Chronological data from Bowring et al. (1998), data with * after Mundil et al. (2004); redox conditions from Shen et al. (2007); high resolution profile and microfossil record modified after Shen et al. (2010).

(Shen et al., 2007; Bond and Wignall, 2010). A land wildfire in the Meishan section, which was revealed by the distributions of PAHs and BC in the sediments, started from the middle of bed 25 and continued into bed 26. This record continues a little later than the mass extinction horizon due to delay effects induced by transportation and deposition after burning. Overall, intensive volcanism, anoxia, mass extinction and wildfires can be integrated together and happened at nearly the same time, with a short time range of <1 Ma (Bowring et al., 1998; Jin et al., 2000; Mundil et al., 2004).

4.3.2. Volcanism

It is well known that the largest continental flood basalt eruption known in geologic history, the Siberian Traps, occurred at the P/Tr boundary (Kamo et al., 2003; Saunders and Reichow, 2009; Svensen et al., 2009). Regionally, there was also widespread intermediate to acidic volcanism in South China (Zhou and Kyte, 1988; Yin et al., 1989; Bowring et al., 1998; Xu et al., 2007; Saunders and Reichow, 2009; Svensen et al., 2009). Volcanic materials indicate that wildfire events at the Meishan P/Tr boundary co-occurred with episodes of the most intensive acidic volcanic activity (Figs. 2k and 8; He et al., 1987; Yin et al., 1989; Shen et al., 2010). The temporal coincidence suggests that wildfire probably resulted from powerful volcanic activities that could provide heat and ignition for combustion. Furthermore, it should be noted that intensive volcanism might greatly change the environmental conditions (Yin et al., 1989; Kamo et al., 2003; Saunders and Reichow, 2009; Svensen et al., 2009) and account for the death of plants. Dead vegetation could be ignited by lightning strikes and the combustion products preserved as an indicator of wildfires (Jones and Lim, 2000; Scott, 2000).

The Siberian Traps probably contributed 20% of the ash in the Meishan P/Tr boundary clay (Xu et al., 2007), and thus it is possible that soot was produced during the intrusion of magma, released with the eruption and transported together with the volcanic ash. Regional volcanic eruptions would also release BC particles, which then settled into sediments in the Meishan section (He et al., 1987; Yin et al., 1989). To truly validate this hypothesis, more sedimentary profiles across the P/Tr boundary from around the world are needed for correlation.

4.3.3. Land hypoxia

Because oxygen is a most important element in combustion, oxygen levels in the atmosphere are likely a significant control on long-term wildfire occurrence (Scott and Glasspool, 2006). Based on experiments, Belcher and McElwain (2008) argued that 17% O_2 in the atmosphere is likely a realistic lower limit for the occurrence of natural wildfires. Hence, the wildfire record in the Meishan area reveals that the P/Tr O_2 concentration in the atmosphere was likely >17% (which is close to the present atmospheric level of O_2), without an obvious deficiency that was previously assumed (Berner, 2005; Huey and Ward, 2005). This measurement coincides with the Glasspool and Scott (2010) result reconstructed from sedimentary charcoal. Moreover, new results using the revised GEOCARBSULF model also showed a high level of O_2 content in the atmosphere (~19%) during the P/Tr boundary (Berner, 2009). This result suggests that hypoxia unlikely played an important role in mass extinctions in terrestrial ecosystems during the P/Tr boundary (Huey and Ward, 2005; Retallack and Jahren, 2008; Glasspool and Scott, 2010).

4.3.4. Marine anoxia

Wildfires on land will destroy vegetation and result in deforestation, which increases erosion and the transfer of land materials (e.g., minerals, plant residues, charcoal, nutrient elements such as N, P, K, etc.) to the marine environment (Kump, 1988; Glasspool, 2000). This process was revealed by an enrichment of dibenzofuran around the P/Tr boundary in the Meishan section, which was likely a degradation product of polysaccharide in soils (Wang and Visscher, 2007). Increasing the input of organic materials and inorganic nutrients, therefore, enhanced both the marine primary productivity and global sequestration of organic carbon burial (Finkelstein et al., 2006), which greatly promoted the development of marine anoxia at the P/Tr boundary as indicated by sedimentary facies (Wignall and Twitchett, 2002), pyrite framboids (Shen et al., 2007), biomarkers and sulfur isotopes (Grice et al., 2005). The anoxic depositional conditions, in contrast, favor long-term preservation of wildfire evidence (Masiello, 2004).

4.3.5. Mass extinction

A wildfire occurred, for example, in Indonesia in 1997–1998. This fire was a significant disaster (32% of the studied area burned) that had important environmental impacts, releasing a total of 0.80–2.57 billion tons of carbon into the air (Page et al., 2002). The wildfire was also a potential source of iron fertilization that could have promoted the extraordinary productivity in upwelled water, which is linked to the death of the coastal reef ecosystem (Abram et al., 2003).

The effects of wildfires, as far as they are known in the Meishan P/Tr section, occurred in parallel to the major extinction process (such as volcanism) and the final resulting event (such as mass extinction). Previous studies have suggested that the wildfire record may be a possible indicator of land mass-extinction (Xie et al., 2007a), but further strata correlation between marine and non-marine sections is needed. As a result, the P/Tr land mass extinction (where the peak of wildfire evidence is in the middle of bed 26) was synchronous with, or occurred a little later than, the marine biota crisis (middle of pyrite crust) in the Meishan section. This delay is conceivable and can be interpreted from the duration of long-distance transportation and deposition.

5. CONCLUSION

To determine whether wildfire activity occurred at the P/Tr boundary in the Meishan section, both PAH concentrations and BC morphology were studied in detail. The elevated concentrations of PAHs near the P/Tr boundary is similar to the BC content distribution, and both reach a peak in concentration in bed 26, which is indicative of P/Tr wildfire events. The prevalence of parent Phe and

the non-metric multidimensional scaling analysis reveal the record of a vegetation-burning wildfire in the Meishan section. BC, seen as irregular charcoal particles to fine soot, usually coexists with pyrite framboids. The equivalent reflectance of the charcoal particles reaches up to 3.5%, which suggests a high combustion temperature of above 500 °C.

Wildfire records were also reported in many other P/Tr sections around the world, and thus wildfires were probably a common phenomenon across the P/Tr transition. High-resolution, integrated profiles support temporal coincidence among intensive volcanism, mass extinction, marine anoxia and wildfires. The occurrence of wildfires suggests that the atmospheric O_2 level at the end of Permian was normal, and no obvious hypoxia occurred on land. The burning of vegetation resulted in land erosion and contributed to the marine anoxia. The co-occurrence of wildfire records and the marine mass extinction suggests that the P/Tr wildfire was a possible proxy for land mass-extinction and provides a direct link between land and marine mass extinction. Therefore, wildfire activity in the Meishan section, revealed by the distributions of PAHs and BC across the P/Tr boundary stratigraphy, provides a novel approach to examine the Earth's greatest mass extinction.

ACKNOWLEDGMENTS

The authors thank Yugan Jin and Hua Zhang for field assistance and additional sample provision, Bixian Mai for supplying standard samples of deuterated PAHs. We are very grateful to Claire M. Belcher for constructive comments and English corrections on the manuscript. Wolf Uwe Reimold (associate editor) and three anonymous reviewers of the paper are gratefully acknowledged for valuable suggestions that greatly improved the manuscript. This study was supported by the Knowledge Innovation Program of Chinese Academy of Sciences (KZCX2-YW-110, KZCX2-YW-Q08-1), National Natural Science Foundation of China (Grant Nos. 40803014, 40972093) and the Fundamental Research Funds for the Central Universities and NSFZJ project (Grant No. R5080124).

REFERENCES

Abram N. J., Gagan M. K., McCulloch M. T., Chappell J. and Hantoro W. S. (2003) Coral reef death during the 1997 Indian ocean dipole linked to Indonesian wildfires. *Science* **301**, 952–955.

Alford J. M., Bernal C., Cates M. and Diener M. D. (2008) Fullerene production in sooting flames from 1,2,3,4-tetrahydronaphthalene. *Carbon* **46**, 1623–1625.

Arinobu T., Ishiwatari R., Kaiho K. and Lamolda M. A. (1999) Spike of pyrosynthetic polycyclic aromatic hydrocarbons associated with an abrupt decrease in delta 13 °C of a terrestrial biomarker at the Cretaceous–Tertiary boundary at Caravaca, Spain. *Geology* **27**, 723–726.

Ascough P. L., Bird M. I., Scott A. C., Collinson M. E., Cohen-Ofri I., Snape C. E. and Le Manquais K. (2010) Charcoal reflectance measurements: implications for structural characterization and assessment of diagenetic alteration. *J. Archaeol. Sci.* **37**, 1590–1599.

Becker L., Poreda R. J., Hunt A. G., Bunch T. E. and Rampino M. (2001) Impact event at the Permian–Triassic boundary: evidence from extraterrestrial noble gases in fullerenes. *Science* **291**, 1530–1533.

Belcher C. M. and McElwain J. C. (2008) Limits for combustion in low O_2 redefine paleoatmospheric predictions for the Mesozoic. *Science* **321**, 1197–1200.

Belcher C. M., Finch P., Collinson M. E., Scott A. C. and Grassineau N. V. (2009) Geochemical evidence for combustion of hydrocarbons during the K–T impact event. *Proc. Natl. Acad. Sci. USA* **106**, 4112–4117.

Berner R. A. (2005) The carbon and sulfur cycles and atmospheric oxygen from middle Permian to middle Triassic. *Geochim. Cosmochim. Acta* **69**, 3211–3217.

Berner R. A. (2009) Phanerozoic atmospheric oxygen: new results using the GEOCARBSULF model. *Am. J. Sci.* **309**, 603–606.

Bond D. P. G. and Wignall P. B. (2010) Pyrite framboid study of marine Permian–Triassic boundary sections: a complex anoxic event and its relationship to contemporaneous mass extinction. *Geol. Soc. Am. Bull.* **122**, 1265–1279.

Bowman D. M. J. S., Balch J. K., Artaxo P., Bond W. J., Carlson J. M., Cochrane M. A., D'Antonio C. M., DeFries R. S., Doyle J. C., Harrison S. P., Johnston F. H., Keeley J. E., Krawchuk M. A., Kull C. A., Marston J. B., Moritz M. A., Prentice I. C., Roos C. I., Scott A. C., Swetnam T. W., van der Werf G. R. and Pyne S. J. (2009) Fire in the Earth system. *Science* **324**, 481–484.

Bowring S. A., Erwin D. H., Jin Y. G., Martin M. W., Davidek K. and Wang W. (1998) U/Pb zircon geochronology and tempo of the end-Permian mass extinction. *Science* **280**, 1039–1045.

Braun T., Osawa E., Detre C. and Toth I. (2001) On some analytical aspects of the determination of fullerenes in samples from the Permian/Triassic boundary layers. *Chem. Phys. Lett.* **348**, 361.

Cao C. and Zheng Q. (2009) Geological event sequences of the Permian–Triassic transition recorded in the microfacies in Meishan section. *Sci. China, Ser. D Earth Sci.* **52**, 1529–1536.

Cao C., Love G. D., Hays L. E., Wang W., Shen S. and Summons R. E. (2009) Biogeochemical evidence for euxinic oceans and ecological disturbance presaging the end-Permian mass extinction event. *Earth Planet. Sci. Lett.* **281**, 188–201.

Cao C., Wang W., Liu L., Shen S. and Summons R. E. (2008) Two episodes of ^{13}C-depletion in organic carbon in the latest Permian: evidence from the terrestrial sequences in northern Xinjiang, China. *Earth Planet. Sci. Lett.* **270**, 251–257.

Chijiwa T., Arai T., Sugai T., Shinohara H., Kumazawa M., Takano M. and Kawakami S.-i. (1999) Fullerenes found in the Permo–Triassic mass extinction period. *Geophys. Res. Lett.* **26**, 767–770.

Diessel C. F. K. (2010) The stratigraphic distribution of inertinite. *Inter. J. Coal Geol.* **81**, 251–268.

Erwin D. H., Bowring S. A. and Jin Y. G. (2002) End-Permian mass extinctions: a review. In *Catastrophic Events and Mass Extinctions: Impacts and Beyond* (eds. C. Koebel and K. G. MacLeod). Boulder, Colorado, Geological Society of America Special Paper 356. pp. 363–383.

Farley K. A., Mukhopadhyay S., Isozaki Y., Becker L. and Poreda R. J. (2001) An extraterrestrial impact at the Permian–Triassic boundary? *Science* **293**, 2343a.

Farley K. A., Ward P., Garrison G. and Mukhopadhyay S. (2005) Absence of extraterrestrial ^{3}He in Permian–Triassic age sedimentary rocks. *Earth Planet. Sci. Lett.* **240**, 265.

Finkelstein D. B., Pratt L. M., Curtin T. M. and Brassell S. C. (2005) Wildfires and seasonal aridity recorded in Late Cretaceous strata from south-eastern Arizona, USA. *Sedimentology* **52**, 587–599.

Finkelstein D. B., Pratt L. M. and Brassell S. C. (2006) Can biomass burning produce a globally significant carbon-isotope

excursion in the sedimentary record? *Earth Planet. Sci. Lett.* **250**, 501–510.

Gerhardt P., Löffler S. and Homann K. H. (1987) Polyhedral carbon ions in hydrocarbon flames. *Chem. Phys. Lett.* **137**, 306–310.

Glasspool I. J. (2000) A major fire event recorded in the mesofossils and petrology of the Late Permian, Lower Whybrow coal seam, Sydney Basin, Australia. *Paleogeogr. Paleoclimatol. Paleoecol.* **164**, 357–380.

Glasspool I. J. and Scott A. C. (2010) Phanerozoic atmospheric oxygen concentrations reconstructed from sedimentary charcoal. *Nat. Geosci.* **3**, 270–630.

Glikson A. Y. (2008) Milestones in the evolution of the atmosphere with reference to climate change. *Aust. J. Earth Sci.* **55**, 125–139.

Grice K., Cao C., Love G. D., Bottcher M. E., Twitchett R. J., Grosjean E., Summons R. E., Turgeon S. C., Dunning W. and Jin Y. (2005) Photic zone euxinia during the Permian–Triassic superanoxic event. *Science* **307**, 706–709.

Grice K., Nabbefeld B. and Maslen E. (2007) Source and significance of selected polycyclic aromatic hydrocarbons in sediments (Hovea-3 well, Perth Basin, Western Australia) spanning the Permian–Triassic boundary. *Org. Geochem.* **38**, 1795–1803.

Harvey M. C., Brassell S. C., Belcher C. M. and Montanari A. (2008) Combustion of fossil organic matter at the Cretaceous–Paleogene (K–P) boundary. *Geology* **36**, 355–358.

He J., Rui L., Chai C. and Ma S. (1987) The latest Permian and earliest Triassic volcanic activities in the Meishan area of Changxing, Zhejiang. *J. Stratigr.* **11**, 194–199.

Hedges J. I., Eglinton G., Hatcher P. G., Kirchman D. L., Arnosti C., Derenne S., Evershed R. P., Kogel-Knabner I., de Leeuw J. W. and Littke R. (2000) The molecularly-uncharacterized component of nonliving organic matter in natural environments. *Org. Geochem.* **31**, 945–958.

Heymann D., Chibante L. P. F., Brooks R. R., Wolbach W. S. and Smalley R. E. (1994) Fullerenes in the Cretaceous–Tertiary boundary layer. *Science* **265**, 645–647.

Heymann D., Jenneskens L. W., Jehlicka J., Koper C. and Vlietstra E. (2003) Terrestrial and extraterrestrial fullerenes. *Fulleren. Nanotub. Carb. Nanostruct.* **11**, 333–370.

Howard J. B., MacKinnon J. T., Makarovsky Y., Lafleur A. L. and Johnson M. E. (1991) Fullerenes C_{60} and C_{70} in flames. *Nature* **352**, 139–141.

Huang X., Jiao D., Lu L., Huang J. and Xie S. (2006) Distribution and geochemical implication of aromatic hydrocarbons across the Meishan Permian–Triassic boundary. *J. China Univ. Geosci.* **17**, 49–54.

Huey R. B. and Ward P. D. (2005) Hypoxia, global warming, and terrestrial late Permian extinctions. *Science* **308**, 398–401.

Jiang C., Alexander R., Kagi R. I. and Murray A. P. (1998) Polycyclic aromatic hydrocarbons in ancient sediments and their relationships to palaeoclimate. *Org. Geochem.* **29**, 1721–1735.

Jin Y. G., Wang Y., Wang W., Shang Q. H., Cao C. Q. and Erwin D. H. (2000) Pattern of marine mass extinction near the Permian–Triassic boundary in South China. *Science* **289**, 432–436.

Jones T. P. and Lim B. (2000) Extraterrestrial impacts and wildfires. *Paleogeogr. Paleoclimatol. Paleoecol.* **164**, 57–66.

Jones T. P., Scott A. C. and Cope M. (1991) Reflectance measurements and the temperature of formation of modern charcoals and implications for studies of fusain. *Bull. Geol. Soc. France* **162**, 193–200.

Kamo S. L., Czamanske G. K., Amelin Y., Fedorenko V. A., Davis D. W. and Trofimov V. R. (2003) Rapid eruption of Siberian flood-volcanic rocks and evidence for coincidence with the Permian–Triassic boundary and mass extinction at 251 Ma. *Earth Planet. Sci. Lett.* **214**, 75–91.

Kennedy I. M. (1997) Models of soot formation and oxidation. *Prog. Energ. Combust.* **23**, 95–132.

Kiehl J. T. and Shields C. A. (2005) Climate simulation of the latest Permian: implications for mass extinction. *Geology* **33**, 757–760.

Koeberl C., Farley K. A., Peucker-Ehrenbrink B. and Sephton M. A. (2004) Geochemistry of the end-Permian extinction event in Austria and Italy: no evidence for an extraterrestrial component. *Geology* **32**, 1053–1056.

Kratschmer W. (2006) Formation of fullerenes. In *Natural Fullerenes and Related Structures of Elemental Carbon* (eds. Frans J. M. Rietmeijer). Springer, Netherlands. pp. 7–29.

Krull E. S., Retallack G. J., Campbell H. J. and Lyon G. L. (2000) $\Delta^{13}C_{org}$ chemostratigraphy of the Permian–Triassic boundary in the Maitai Group, New Zealand: evidence for high-latitudinal methane release. *N. Z. J. Geol. Geophy.* **43**, 21–32.

Kruskal J. B. (1964) Multidimensional scaling by optimizing goodness of fit to a nonmetric hypothesis. *Psychometrika* **29**, 1–27.

Kump L. R. (1988) Terrestrial feedback in atmospheric oxygen regulation by fire and phosphorus. *Nature* **335**, 152–154.

Li C.-T., Mi H.-H., Lee W.-J., You W.-C. and Wang Y.-F. (1999) PAH emission from the industrial boilers. *J. Hazard. Mater.* **69**, 1–11.

Li Y., Liang H., Yin H., Sun J., Cai H. a., Zhu R. and Ran F. (2005) Determination of fullerenes (C_{60}/C_{70}) from the Permian–Triassic boundary in the Meishan section of south China. *Acta Geol. Sin-Engl.* **79**, 11–15.

Lu L. and Tong J. (2002) Alkane biomarkers in Permian–Triassic boundary strata at Meishan section, Changxing, Zhejiang province. *J. China Univ. Geosci.* **13**, 177–181.

Marlon J. R., Bartlein P. J., Walsh M. K., Harrison S. P., Brown K. J., Edwards M. E., Higuera P. E., Power M. J., Anderson R. S., Briles C., Brunelle A., Carcaillet C., Daniels M., Hu F. S., Lavoie M., Long C., Minckley T., Richard P. J. H., Scott A. C., Shafer D. S., Tinner W., Umbanhowar C. E. and Whitlockg C. (2009) Wildfire responses to abrupt climate change in North America. *Proc. Natl. Acad. Sci. USA* **106**, 2519–2524.

Marynowski L. and Simoneit B. R. T. (2009) Widespread upper Triassic to lower Jurassic wildfire records from Poland: evidence from charcoal and pyrolytic polycyclic aromatic hydrocarbons. *Palaios* **24**, 785–798.

Masiello C. A. (2004) New directions in black carbon organic geochemistry. *Mar. Chem.* **92**, 201–213.

Masiello C. A. and Druffel E. R. M. (1998) Black carbon in deep-sea sediments. *Science* **280**, 1911–1913.

McParland L. C., Collinson M. E., Scott A. C., Steart D. C., Grassineau N. V. and Gibbons S. J. (2007) Ferns and fires: experimental charring of ferns compared to wood and implications for paleobiology, paleoecology, coal petrology, and isotope geochemistry. *Palaios* **22**, 528–538.

McParland L., Collinson M., Scott A. and Campbell G. (2009) The use of reflectance values for the interpretation of natural and anthropogenic charcoal assemblages. *Archaeol. Anthropol. Sci.* **1**, 249–261.

Meyer K. M., Kump L. R. and Ridgwell A. (2008) Biogeochemical controls on photic-zone euxinia during the end-Permian mass extinction. *Geology* **36**, 747–750.

Mundil R., Ludwig K. R., Metcalfe I. and Renne P. R. (2004) Age and timing of the Permian mass extinctions: U/Pb dating of closed-system zircons. *Science* **305**, 1760–1763.

Nabbefeld B., Grice K., Summons R. E., Hays L. E. and Cao C. (2010) Significance of polycyclic aromatic hydrocarbons

(PAHs) in Permian/Triassic boundary sections. *Appl. Geochem.* **25**, 1374–1382.

Oros D. R. and Simoneit B. R. T. (2000) Identification and emission rates of molecular tracers in coal smoke particulate matter. *Fuel* **79**, 515–536.

Oros D. R. and Simoneit B. R. T. (2001) Identification and emission factors of molecular tracers in organic aerosols from biomass burning. Part 1: Temperate climate conifers. *Appl. Geochem.* **16**, 1513–1544.

Page S. E., Siegert F., Rieley J. O., Boehm H.-D. V., Jaya A. and Limin S. (2002) The amount of carbon released from peat and forest fires in Indonesia during 1997. *Nature* **420**, 61–65.

Pancost R. D., Steart D. S., Handley L., Collinson M. E., Hooker J. J., Scott A. C., Grassineau N. V. and Glasspool I. J. (2007) Increased terrestrial methane cycling at the Palaeocene–Eocene thermal maximum. *Nature* **449**, 332–335.

Retallack G. J. and Jahren A. H. (2008) Methane release from igneous intrusion of coal during Late Permian extinction events. *J. Geol.* **116**, 1–20.

Retallack G. J., Metzger C. A., Greaver T., Jahren A. H., Smith R. M. H. and Sheldon N. D. (2006) Middle-late Permian mass extinction on land. *Geol. Soc. Am. Bull.* **118**, 1398–1411.

Saunders A. and Reichow M. (2009) The Siberian Traps and the end-Permian mass extinction: a critical review. *Chin. Sci. Bull.* **54**, 20–37.

Scott A. C. (2000) The pre-Quaternary history of fire. *Paleogeogr. Paleoclimatol. Paleoecol.* **164**, 281–329.

Scott A. C. (2010) Charcoal recognition, taphonomy and uses in palaeoenvironmental analysis. *Paleogeogr. Paleoclimatol. Paleoecol.* **291**, 11–39.

Scott A. C. and Damblon F. (2010) Charcoal: taphonomy and significance in geology, botany and archaeology. *Paleogeogr. Paleoclimatol. Paleoecol.* **291**, 1–10.

Scott A. C. and Glasspool I. J. (2005) Charcoal reflectance as a proxy for the emplacement temperature of pyroclastic flow deposits. *Geology* **33**, 589–592.

Scott A. C. and Glasspool I. J. (2006) The diversification of Paleozoic fire systems and fluctuations in atmospheric oxygen concentration. *Proc. Natl. Acad. Sci. USA* **103**, 10861–10865.

Scott A. C. and Jones T. P. (1994) The nature and influence of fire in Carboniferous ecosystems. *Paleogeogr. Paleoclimatol. Paleoecol.* **106**, 91–112.

Scott A. C., Kenig F., Plotnick R. E., Glasspool I. J., Chaloner W. G. and Eble C. F. (2010) Evidence of multiple late Bashkirian to early Moscovian (Pennsylvanian) fire events preserved in contemporaneous cave fills. *Paleogeogr. Paleoclimatol. Paleoecol.* **291**, 72–84.

Shen W. J. and Lin Y. T. (2010) Environmental conditions and events prior to the Permian–Triassic boundary at Meishan section, China. *J. Earth Sci.* **21**, 151–153.

Shen W., Lin Y., Wang D., Zhou Y. and Miao B. (2006) Advances in the study of natural fullerenes with special discussion on P–T boundary fullerene. *Adv. Earth Sci.* **21**, 903–910.

Shen W., Lin Y., Xu L., Li J., Wu Y. and Sun Y. (2007) Pyrite framboids in the Permian–Triassic boundary section at Meishan, China: evidence for dysoxic deposition. *Paleogeogr. Paleoclimatol. Paleoecol.* **253**, 323–331.

Shen W., Lin Y., Sun Y., Xu L. and Zhang H. (2008) Black carbon record across the Permian–Triassic boundary section at Meishan, Changhsing County, Zhejiang Province and its significance. *Acta Petrol. Sin.* **24**, 2407–2414.

Shibuya M., Kato M., Ozawa M., Fang P. H. and Osawaa E. (1999) Detection of buckminsterfullerene in usual soots and commercial charcoals. *Fullerene Sci. Techn.* **7**, 181–193.

Simoneit B. R. T. (2002) Biomass burning – a review of organic tracers for smoke from incomplete combustion. *Appl. Geochem.* **17**, 129–162.

Summons R. E. and Powell T. G. (1986) Chlorobiaceae in Palaeozoic seas revealed by biological markers, isotopes and geology. *Nature* **319**, 763–765.

Svensen H., Planke S., Polozov A. G., Schmidbauer N., Corfu F., Podladchikov Y. Y. and Jamtveit B. (2009) Siberian gas venting and the end-Permian environmental crisis. *Earth Planet. Sci. Lett.* **277**, 490–500.

Thomas B. M., Willink R. J., Grice K., Twitchett R. J., Purcell R. R., Archbold N. W., George A. D., Tye S., Alexander R., Foster C. B. and Barber C. J. (2004) Unique marine Permian–Triassic boundary section from Western Australia. *Aust. J. Earth Sci.* **55**, 423–430.

Uhl D. and Montenari M. (2010) Charcoal as evidence of palaeowildfires in the Late Triassic of SW Germany. *Geol. J.* doi: 10.1002/gj.1229.

Uhl D., Abu Hamad A., Kerp H. and Bandel K. (2007) Evidence for palaeo-wildfire in the Late Permian palaeotropics – charcoalified wood from the Um IRNA formation of Jordan. *Rev. Palaeobot. Palyno.* **144**, 221–230.

Venkatesan M. I. and Dahl J. (1989) Organic geochemical evidence for global fires at the Cretaceous/Tertiary boundary. *Nature* **338**, 57–60.

Wang C. (2007) Anomalous hopane distributions at the Permian–Triassic boundary, Meishan, China – evidence for the end-Permian marine ecosystem collapse. *Org. Geochem.* **38**, 52–66.

Wang C. and Visscher H. (2007) Abundance anomalies of aromatic biomarkers in the Permian–Triassic boundary section at Meishan, China – evidence of end-Permian terrestrial ecosystem collapse. *Paleogeogr. Paleoclimatol. Paleoecol.* **252**, 291–303.

Wang S. and Yin H. (2001) *Study on terrestrial Permian–Triassic boundary strata in East Yunnan and West Guizhou*. Press of China University of Geosciences, Wuhan.

Wang Z.-q. and Chen A.-s. (2001) Traces of arborescent lycopsids and dieback of the forest vegetation in relation to the terminal Permian mass extinction in North China. *Rev. Palaeobot. Palyno.* **117**, 217–243.

Wignall P. B. (2001) Large igneous provinces and mass extinctions. *Earth-Sci. Rev.* **53**, 1–33.

Wignall P. B. and Twitchett R. J. (2002) Extent, duration, and nature of the Permian–Triassic superanoxic event. In *Catastrophic Events and Mass Extinctions: Impacts and Beyond* (eds. C. Koebel and K. G. MacLeod). Boulder, Colorado: Geological Society of America Special Paper 356. pp. 395–413.

Wildman, Jr., R. A., Hickey L. J., Dickinson M. B., Berner R. A., Robinson J. M., Dietrich M., Essenhigh R. H. and Wildman C. B. (2004) Burning of forest materials under late Paleozoic high atmospheric oxygen levels. *Geology* **32**, 457–460.

Xie S., Pancost R. D., Yin H., Wang H. and Evershed R. P. (2005) Two episodes of microbial change coupled with Permo/Triassic faunal mass extinction. *Nature* **434**, 494–497.

Xie S., Pancost R. D., Huang J., Wignall P. B., Yu J., Tang X., Chen L., Huang X. and Lai X. (2007a) Changes in the global carbon cycle occurred as two episodes during the Permian Triassic crisis. *Geology* **35**, 1083–1086.

Xie S., Pancost R. D., Huang X., Jiao D., Lu L., Huang J., Yang F. and Evershed R. P. (2007b) Molecular and isotopic evidence for episodic environmental change across the Permo/Triassic boundary at Meishan in South China. *Glob. Planet. Change* **55**, 56–65.

Xu L., Lin Y., Shen W., Qi L., Xie L. and Ouyang Z. (2007) Platinum-group elements of the Meishan Permian–Triassic boundary section: evidence for flood basaltic volcanism. *Chem. Geol.* **246**, 55–64.

Xu S. and Sun Y. (2006) Micro-column chromatography for the separation of compound-grouped fractions of sedimentary organic matter. *Geochimica* **35**, 681–688.

Yin H., Tong J. and Zhang K. (2005) A review on the global stratotype section and point of the Permian–Triassic boundary. *Acta Geol. Sin-Engl.* **79**, 715–728.

Yin H., Huang S., Zhang K., Yang F., Ding M., Bi X. and Zhang S. (1989) Volcanism at the Permian–Triassic boundary in south China and its effects on mass extinction. *Acta Geol. Sin-Chinese* **63**, 169–180.

Yin H., Zhang K., Tong J., Yang Z. and Wu S. (2001) The global stratotype section and point of the Permian–Triassic boundary (GSSP). *Episodes* **24**, 102–114.

Yin H., Feng Q., Lai X., Baud A. and Tong J. (2007) The protracted Permo–Triassic crisis and multi-episode extinction around the Permian–Triassic boundary. *Glob. Planet. Change* **55**, 1–20.

Zhou L. and Kyte F. T. (1988) The Permian–Triassic boundary event: a geochemical study of three Chinese sections. *Earth Planet. Sci. Lett.* **90**, 411–421.

Associate editor: W. Uwe Reimold